Macromolecules

pubs.acs.org/Macromolecules Article

Tailoring Dynamic Chiral Supramolecular Assembly with Phototriggered Radical Anions of C_3-Symmetric Triphenylene Triimides

Namhee Kim, Jun Su Kang, Taesuk Jun, Jong-Min Suh, Deok-Ho Roh, Won-Woo Park, Oh-Hoon Kwon, Tae-Hyuk Kwon, Mi Hee Lim, Du Yeol Ryu, Myungeun Seo, and Byeong-Su Kim*

Cite This: https://doi.org/10.1021/acs.macromol.3c01189 Read Online

ACCESS | Metrics & More | Article Recommendations | Supporting Information

ABSTRACT: This study develops a new type of C_3-symmetric triphenylene triimide (TTI) bearing different oligo(ethylene glycol) side chains via imide linkages. By exploiting the unique TTI molecule as a building block, supramolecular polymerization is explored based on $\pi-\pi$ stacking and hydrophilic/hydrophobic interactions in various solvents and the rates of heating/cooling process. The molecular chirality of the TTI unimer induces a preferential helicity formation in fibrous structures, while the achiral side chain allows the formation of linear nanofibers. The stacking type of supramolecular polymerization is highly dependent on the point chirality of the side chains, as indicated by the spectroscopic analyses, including ultraviolet−visible (UV/vis) and circular dichroism (CD) spectroscopy with atomic force microscopy (AFM), transmission electron microscopy (TEM), and wide-angle X-ray scattering (WAXS). Interestingly, the supramolecular polymerization does not occur in its monomeric state due to the generation of radical anions from the imide groups upon UV irradiation. In contrast, the fibrous structure in the assembled state is maintained, owing to the intermolecular interaction. This study provides a new direction in the phototriggered control of the supramolecular chiral assembly.

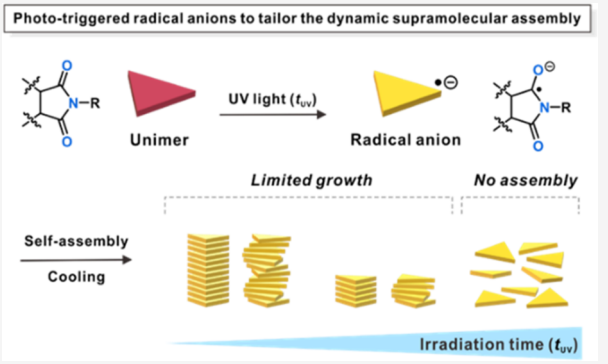

1. INTRODUCTION

Over the past three decades, supramolecular polymers have attracted considerable attention owing to their ability to produce responsive, reconfigurable, and recyclable functional structures with the potential to regulate structural dynamics.[1] Inspired by the homochirality of biological macromolecules such as proteins and polynucleic acids, chiral supramolecular assemblies have emerged as artificial systems that can mimic biological structures.[2,3] Chiral supramolecular polymers can display significant potentials in chiral detection,[4,5] asymmetric catalysts,[6−8] chiral optoelectronics,[9−12] and the realization of biological functions. Chiral information can be transferred from the molecular level to the macroscopic level via noncovalent interactions between repeating units such as hydrogen bonding, $\pi-\pi$ stacking, van der Waals interaction, hydrophobic interaction, and electrostatic interaction. The chirality of supramolecular polymers is mainly induced by intrinsic molecular chirality[13,14] or external stimuli, such as circularly polarized light[15,16] and chiral solvents.[17,18] Among various chiral sources, molecular chirality is imparted to molecular structures by introducing point, axial, or helical chirality without the use of specific chemical moieties or reagents. Under different environments, chiral molecules with asymmetric spatial structures can be aggregated into chiral supramolecular polymers with diverse stacking types such as helices,[19,20] superhelices,[21,22] and twisted lamellae.[23,24]

Due to the reversibility in noncovalent bonding, supramolecular polymers are in thermodynamic equilibrium. Therefore, the self-assembly process is primarily regulated by external environmental factors, such as the solvent,[25,26] temperature,[27,28] metal ion,[29,30] and light.[30,31] Among these factors, light is extensively employed as a nondestructive stimulus owing to its high spatiotemporal control, facile processing, and fast read out.[32] Supramolecular polymers of photochromic compounds, such as azobenzene[33−36] and diarylethene[37−40] derivatives, exhibit unique phototriggered isomerization. These photoresponsive properties have attracted much attention due to their dynamic influence on the stacking/polymerization process to modulate morphology.

Received: June 19, 2023
Revised: November 14, 2023
Accepted: December 15, 2023

Scheme 1. (a) Synthetic Steps and Molecular Structures of *N*-TTI, *R*-TTI, and *S*-TTI. (b) Supramolecular Polymerization Process (Top) and Radical-Mediated Structure Variation under UV Light Irradiation (365 nm) (Bottom)

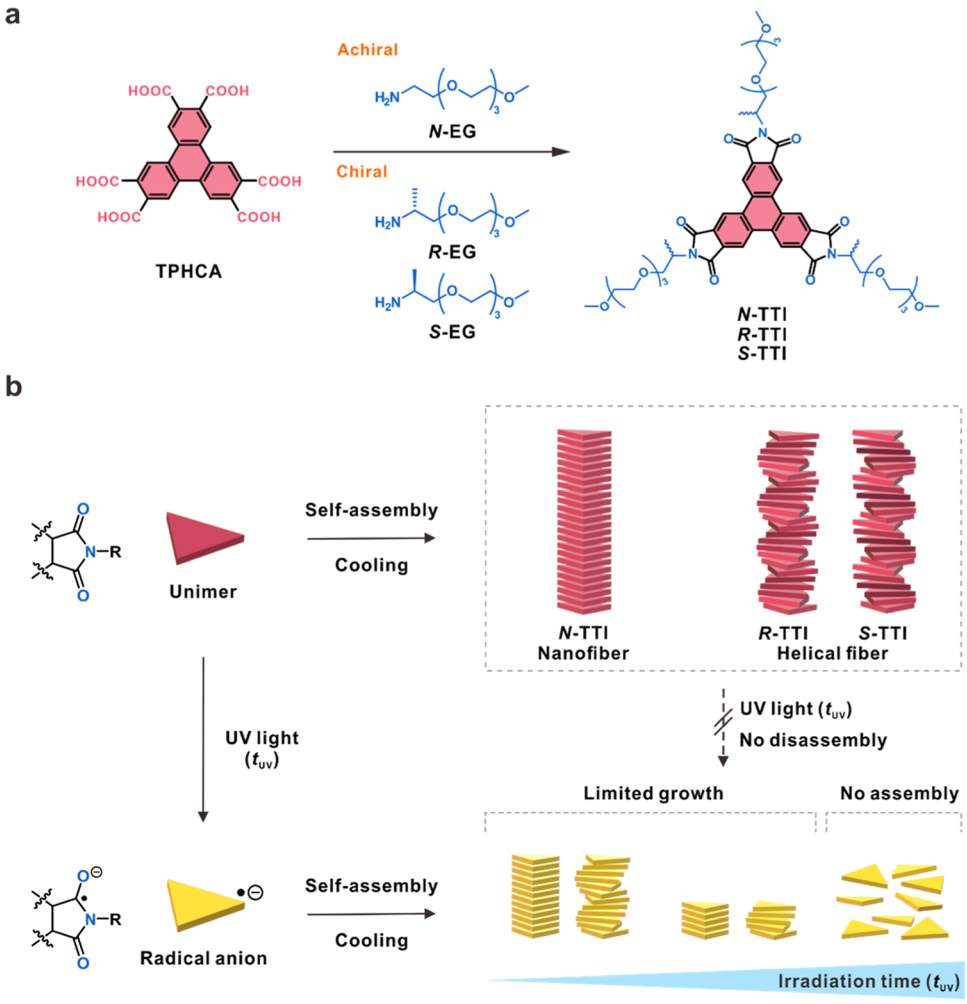

In this context, aromatic imide compounds, such as perylene diimides[41−44] and naphthalene diimides,[45−48] have unique photoresponsive properties that produce radical anions under different stimuli, including treatment with a reducing agent,[49,50] electrochemical reduction,[51,52] and light.[42,53] The radical anion formed in the imide group is stabilized by the delocalization of spin and charge due to the presence of the carbonyl group and aromatic core.[46,54,55] Despite the rich literature on the phototriggered formation of radical anions, few studies have shown that the formation of radical anions in aromatic imide compounds has a dynamic effect on the supramolecular assembly process.[46,49,53] For example, the radical anions generated from a perylene diimide derivative using a reducing agent induced the disassembly of supramolecular polymers.[49] Meanwhile, the radical anions produced from a naphthalene diimide derivative via light irradiation exhibited enhanced circularly polarized luminescence while maintaining its supramolecular structure.[53] It is known that radical anions assemble into aggregates in naphthalene diimide systems.[51,52] These findings highlight the need to investigate the effect of radical anions on the dynamic self-assembly and disassembly processes of aromatic imide-based supramolecular polymers.

Herein, we report the synthesis, self-assembly, and photoresponsive properties of unique triphenylene triimides compounds. The chemical structures of achiral and chiral C_3-symmetric triphenylene triimides (*N*-TTI, *R*-TTI, and *S*-TTI) are shown in Scheme 1a. The building blocks comprise a conjugated triphenylene core and three oligo(ethylene glycol) (OEG) chains. The molecular chirality of *R*/*S*-TTI is considered to pose a point chirality in the OEG chains. The aromatic core unit and polar side chain can induce $\pi-\pi$ stacking and hydrophilic−hydrophobic interactions, respectively. An imide bond was introduced as a linker between the core and peripheral units because its photoresponsive properties regulate the self-assembly process. In the monomeric state, ultraviolet (UV) irradiation caused the formation of radical anions in the aromatic imide units, limiting the continuous growth by generating deactivated unimers. On the contrary, UV irradiation in the assembled state maintained its fibrous structure owing to the presence of strong intermolecular interactions.

2. RESULTS AND DISCUSSION

Initially, the core unit and side chains were prepared and characterized using ^{1}H NMR spectroscopy (see Schemes S1−S3 and Figures S1−S4 in the Supporting Information). Subsequently, *N*-TTI, *R*-TTI, and *S*-TTI unimers were synthesized through a simple one-step condensation reaction to form an imide group from the triphenylene dicarboxylic acid

https://doi.org/10.1021/acs.macromol.3c01189
Macromolecules XXXX, XXX, XXX−XXX

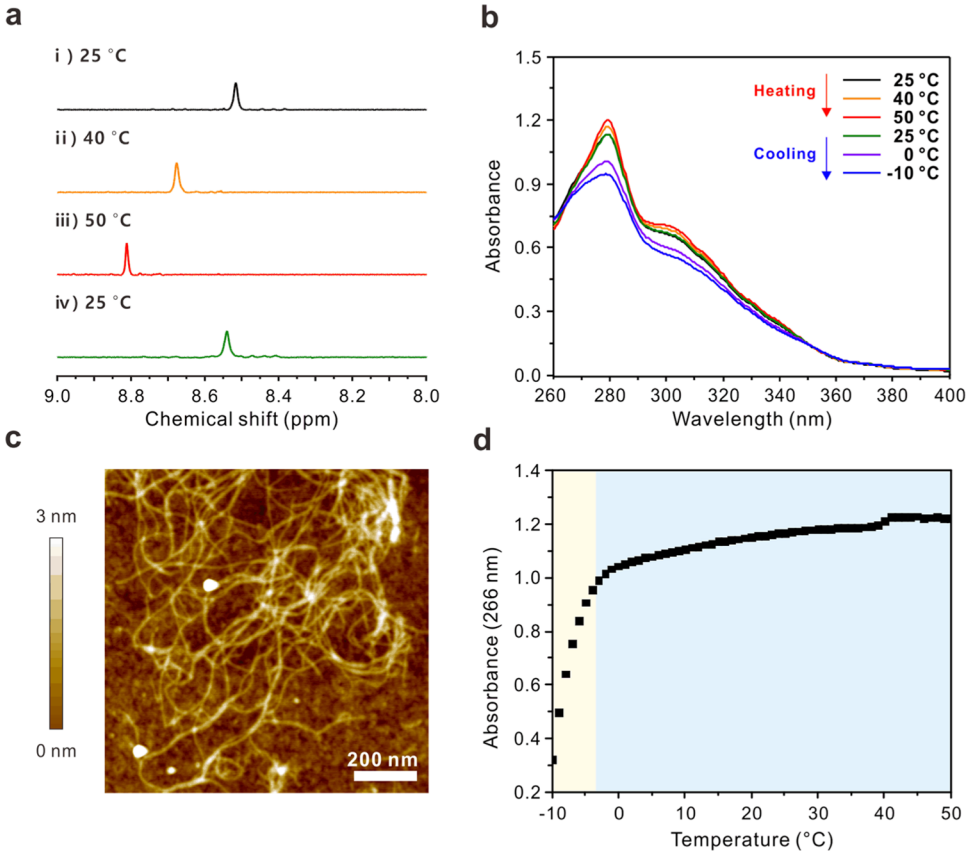

Figure 1. (a) Variable-temperature ^{1}H NMR spectra of *N*-TTI (0.10 wt % in methanol-d_4). (b) UV−vis absorption spectra of *N*-TTI with varying temperatures (0.01 wt % in methanol). (c) Representative height-mode AFM image of *N*-TTI spin coated on a silicon wafer substrate (0.01 wt % in methanol). (d) Absorbance of *N*-TTI at λ = 266 nm with temperature variations at a cooling rate of 1 K/min.

and corresponding OEG amines (Scheme 1a). The resulting series of TTI compounds were successfully characterized using ^{1}H and ^{13}C NMR spectroscopy, mass spectrometry, and Fourier transform infrared (FT-IR) spectroscopy confirming the formation of the desired achiral and chiral unimers (Figures S5−S13).

A supramolecular polymer was obtained by slowly cooling the alcoholic solution of each *N*/*R*/*S*-TTI unimer so that the unimers could grow uniformly during the self-assembly process. While the achiral *N*-TTI unimers self-assembled into linear nanofibers, the chiral *R*-TTI and *S*-TTI unimers self-assembled into helical supramolecular polymers (Scheme 1b). A variable-temperature ^{1}H NMR (VT-NMR) experiment was performed in deuterated methanol to confirm the aggregation behavior of the *N*-TTI unimer (Figure 1a). The peak intensity of the aromatic protons increased gradually with a decreasing peak width as the *N*-TTI unimer solution was heated from 25 to 50 °C, indicating the presence of aggregated species. These temperature-dependent changes were also reversible upon temperature cycling between 25 and 50 °C. A downfield shift for the aromatic proton signal from 8.51 ppm at 25 °C to 8.81 ppm at 50 °C was attributed to the deshielding effect of π electrons due to the small intermolecular distance between adjacent molecules, consistent with the transition from the aggregated state to the unimer state. The decrease in diffusion coefficient (D) observed in DOSY NMR spectra as the temperature decreases provides evidence for the self-aggregation of *N*-TTI in methanol (Figure S14a−c). Moreover, in methanol as a poor solvent, the *N*-TTI solution exhibited opacity at 25 °C, but became transparent at 50 °C, indicating the presence of self-aggregation (Figure S14d). In contrast, no noticeable changes in transparency were observed as the temperature varied in a good solvent such as chloroform. It is confirmed that the $\pi-\pi$ stacking between the aromatic core units is one of the main driving forces in the self-assembly process. The position and width of proton peaks corresponding to the OEG chains changed marginally, indicating that hydrophilic−hydrophobic and van der Waals interactions are involved in the self-assembly process (Figure S15).

Moreover, the self-assembly behavior of *N*-TTI can be examined using variable-temperature UV/vis spectroscopy (VT-UV/vis), which is a useful method for determining the supramolecular polymerization mechanism of aromatic compounds and distinguishing the growth processes based on either isodesmic or cooperative models[56] (Figure 1b). The UV−vis absorption spectrum of *N*-TTI measured at 25 °C comprised two major absorption bands in a methanol solvent: one around 279 nm derived from the triphenylene moiety and one around approximately 300 nm derived from the aromatic imide moiety. Upon heating the solution from 25 to 50 °C, the absorbance increased continuously owing to the dissociation of aggregated structures into monomer structures. However, the absorbance decreased considerably at temperatures as low as −10 °C, which is a characteristic of the transition from the monomers to the aggregation state due to the intermolecular interactions between the building blocks.

Atomic force microscopy (AFM) images of the *N*-TTI assemblies transferred from the cooled methanol solution onto

https://doi.org/10.1021/acs.macromol.3c01189
Macromolecules XXXX, XXX, XXX−XXX

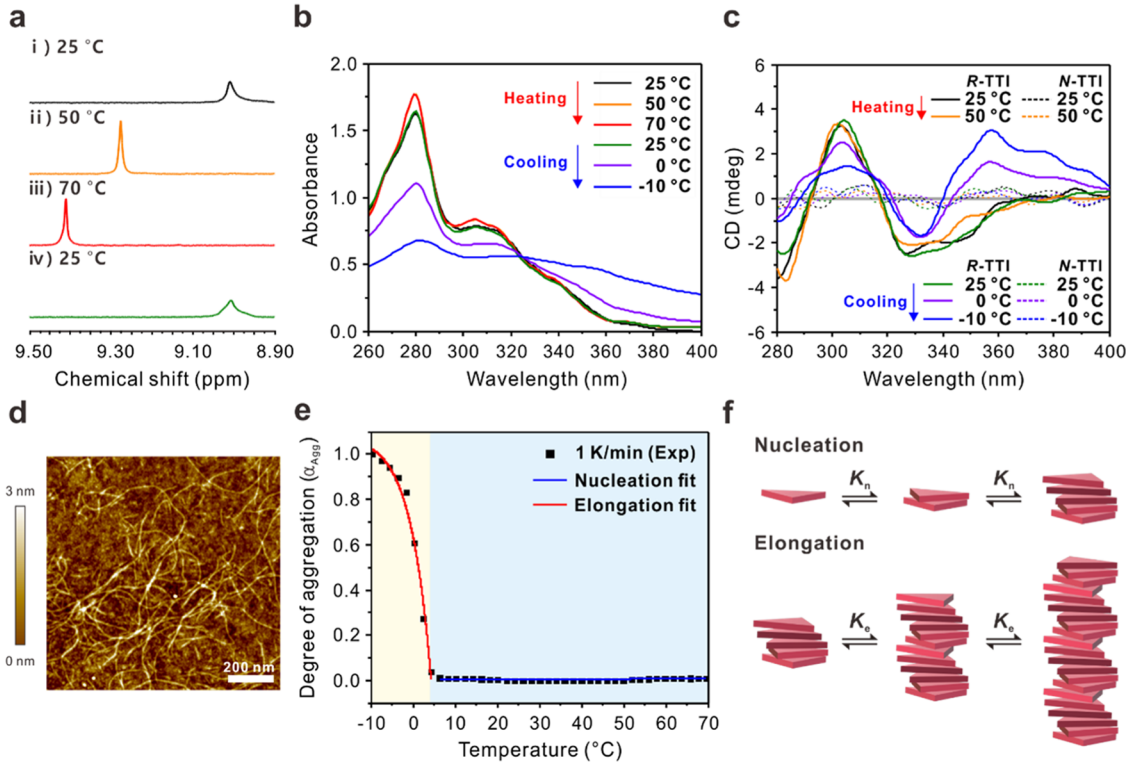

Figure 2. (a) Variable-temperature ^{1}H NMR spectra of *R*-TTI (0.30 wt % in isopropanol-d_8). (b) UV−vis absorption spectra of *R*-TTI with varying temperatures in isopropanol solution (0.03 wt %). (c) Circular dichroism (CD) spectral changes of *R*-TTI and *N*-TTI with varying temperatures. (d) Representative height-mode AFM image of *R*-TTI (0.03 wt %) spin coated from the isopropanol solution on a silicon wafer substrate. (e) Temperature-dependent degree of aggregation (α_{Agg}) of *R*-TTI calculated from the absorption coefficients at λ = 380 nm at a rate of 1 K/min. The degree of aggregation (α_{Agg}) was fitted with a cooperative model. (f) Schematic representation of the supramolecular polymerization process via slow cooling for *R*-TTI. See the self-assembly data of *S*-TTI in the Supporting Information.

a silicon substrate via spin coating showed the presence of nanofibers and some aggregated particles (Figure S16). To prevent random self-assembly, the unimer solution was slowly cooled to −18 °C at a rate of 1 K/min. Hence, the AFM image of the solution shows well-ordered nanofibers with a uniform average diameter of 22.2 ± 1.6 nm (Figure 1c).

The changes in absorbance with temperature reveal a gradual decline at higher temperatures followed by a steep drop below a specific temperature (Figure 1d). This alteration in absorbance with temperature unmistakably signifies the presence of intermolecular interactions. While the measurement of absorbance values below −10 °C was unattainable due to instrumental limitation, we performed the model fitting for quantitative analysis by assuming a degree of aggregation (α_{Agg}) of 1 at −10 °C. Specifically, the degree of aggregation (α_{Agg}) of *N*-TTI is calculated from the change in the absorption coefficients at 266 nm with respect to temperature (cooling process) (Figure S17 and Table S1).[18] Nonsigmoidal curves were obtained at the rates of 1 K/min, clearly indicating the characteristic of cooperative supramolecular polymerization mechanism with nucleation elongation. The cooperative fitting matched the data, whereas the isodesmic fitting failed. The elongation temperature of *N*-TTI at 1 K/min was noted at −4 °C. On the other hand, upon cooling from 50 to −10 °C at a rate of 10 K/min, only the nucleation step was present without the elongation step (Figure S18). The elongation temperature of *N*-TTI at a cooling rate of 10 K/min is expected to be lower than −10 °C, which is below the instrumental limit. During fast cooling, it is difficult to keep up with the temperature change, and hence, the elongation temperature is inevitably lowered.

Similar to the analysis of *N*-TTI, we performed the characterization of the assembly of *R*-TTI and *S*-TTI. Since the VT-UV/vis spectra established that the assembly behavior of *R*-TTI was not clearly shown in methanol, the self-assembly was performed in isopropanol to match the solubility of less polar unimers due to the presence of a chiral methyl group in the side chain.

Figure 2a represents the VT-NMR spectra of *R*-TTI collected at different temperatures. A weak and broad peak of the aromatic protons was observed at 25 °C because intermolecular aggregation limited the molecular mobility. However, the peak intensity increased sharply upon heating, resulting from the disassembly into unimers. In addition, the position and width of proton peaks corresponding to OEG chains and methoxy groups changed considerably (Figure S19). These results imply that the noncovalent interactions, including $\pi-\pi$ stacking, hydrophilic−hydrophobic interactions, and van der Waals forces, exist between the *R*-TTI unimers. The change in the absorbance of *R*-TTI assemblies in isopropanol solvent depending on the temperature changes was consistent with the tendency observed in *N*-TTI assemblies. For chloroform as a good solvent for *R*-TTI, it was observed that the absorbance did not decrease with decrease in temperature, indicating the absence of *R*-TTI assemblies (Figure S20a). However, unlike *N*-TTI assemblies, a new absorption band was generated in the red-shifted region upon cooling from 70 to −10 °C (Figure 2b). Similarly, the fluorescence spectra of *R*-TTI exhibited emission in the red-

https://doi.org/10.1021/acs.macromol.3c01189
Macromolecules XXXX, XXX, XXX−XXX

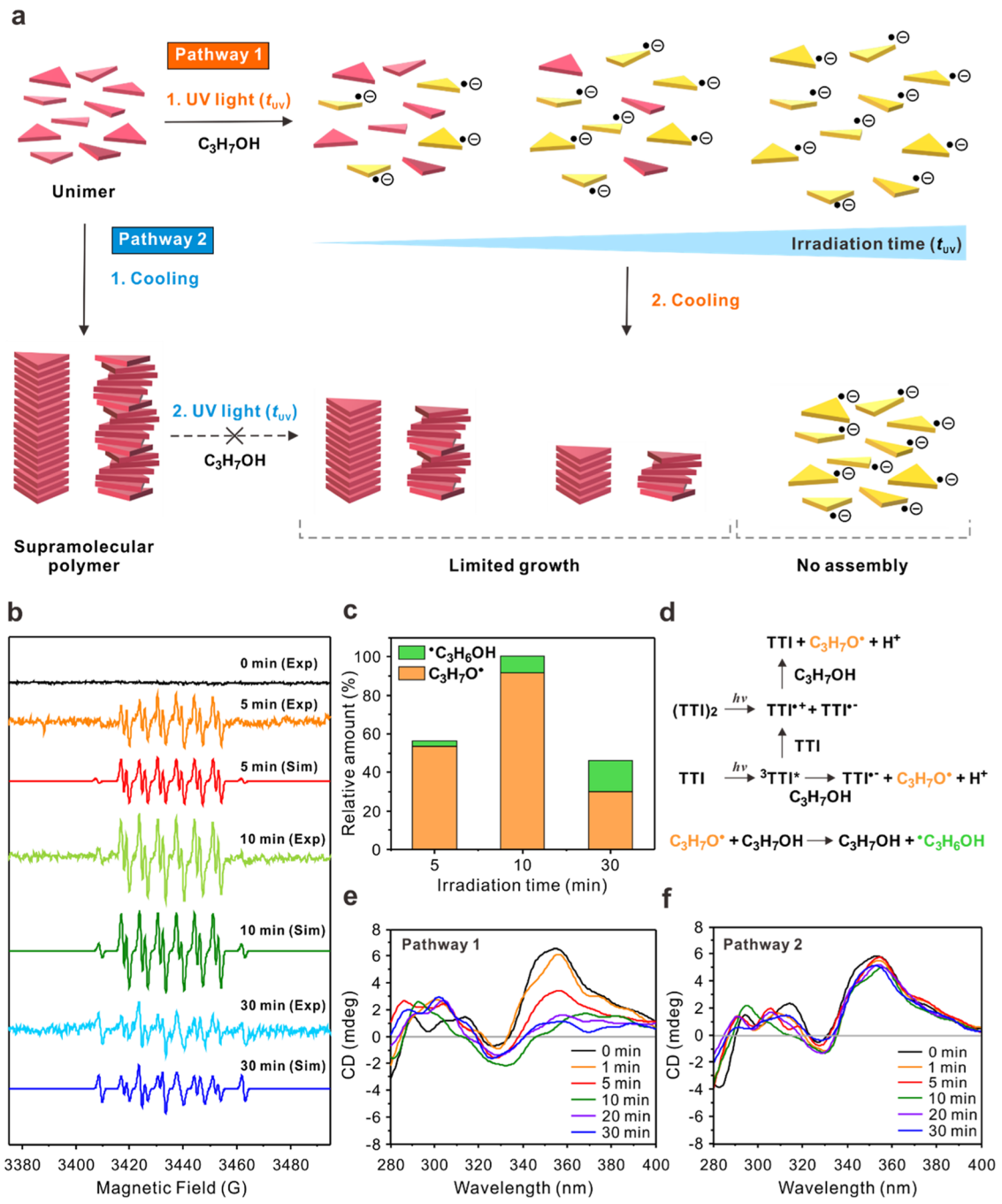

Figure 3. (a) Schematic representation of the radical-mediated structure variation process under UV light irradiation. (b) Experimental and simulated EPR spectra during UV irradiation of *R*-TTI (0.03 wt %) in the presence of 5,5-dimethyl-1-pyrroline *N*-oxide (DMPO) (~50 equiv) in N_2-saturated isopropanol. (c) Relative amounts of DMPO/$^{\bullet}C_3H_6OH$ radicals and DMPO/$C_3H_7O^{\bullet}$ radicals generated for different irradiation times. (d) Possible mechanisms for the formation of radical species under UV irradiation of *R*-TTI in isopropanol solvent. (e) CD spectra of postassembled *R*-TTI unimer after different UV irradiation time. (f) CD spectra of preassembled *R*-TTI assemblies under different UV irradiation time.

shifted region at low temperatures. The broader and decreased fluorescence intensity at lower temperatures indicates the presence of *H*-type aggregated species (Figure S21).[57,58]

Circular dichroism (CD) spectroscopic measurements were conducted to reveal the features of chirality in the *R*-TTI assemblies. Figure 2c shows bisignate CD signals for self-assembled structures at temperatures below 0 °C. No CD signals of *N*-TTI were detected in all of the temperature ranges tested. The Cotton effect was observed with two positive peaks at 305 and 356 nm and a negative peak at 332 nm. Upon decreasing the temperature, the CD signals in the range of 332−400 nm were found to increase and occur below 0 °C, whereas the CD signals in the range of 280−331 nm decreased. The CD signal in the range of 332−400 nm, which occurs during self-assembly at lower temperatures, corresponds to the absorption band of $\pi-\pi^*$ transitions. In chloroform, the CD signal remained consistent in the range of 280−320 nm irrespective of temperature, indicating that it originated from molecular chirality (Figure S20b). Therefore, the CD signals in the range of 280−331 and 332−400 nm were attributed to the

https://doi.org/10.1021/acs.macromol.3c01189
Macromolecules XXXX, XXX, XXX−XXX

dominance of the monomeric and assembled states, respectively. The point chirality was transferred to the triphenylene core in the monomeric state and then aggregation occurred in the cooling process, resulting in the *H*-band in the CD signals. The *S*-TTI self-assembly was characterized by using VT-NMR and VT-UV/vis spectroscopies (Figure S22a,b). The CD spectra of the *R*-TTI and *S*-TTI assemblies displayed mirror images of each other, indicating an apparent enantiomeric relationship (Figure S22c). In particular, the similarity in the trends of changes in absorbance with temperature for *R*-TTI and *S*-TTI indicates that their self-assembly behaviors align with each other despite their opposite chirality (Figure S23). The AFM image of *R*-TTI assemblies showed well-defined nanofibers with a uniform average diameter of 23.7 ± 1.6 nm similar to that for *N*-TTI assemblies (Figure 2d). Unfortunately, because the supramolecular chirality of *R*-TTI was as low as the molecular chirality in the CD spectrum, it was difficult to observe the helical structures in the AFM image. The transmission electron microscopy (TEM) images of the *N*-TTI assemblies showed straight nanofibers with a diameter of 20−50 nm (Figure S24a−c). The length of the nanofibers was in the range of 5−10 μm. The TEM images of the *R*-TTI and *S*-TTI assemblies also exhibited the presence of rigid nanofibers, accompanied by partially distorted twisting and bending features (Figure S24d−i).

The absorption band at 380 nm was monitored as a function of temperature at a rate of 0.5−10 K/min to obtain the specific temperature at which the assemblies began to grow (Figure S25). These abrupt changes are typically observed in cooperative supramolecular polymerization with nucleation and elongation stages (Figure 2f). Indeed, the cooperative fitting successfully matched the data, while the isodesmic fitting failed (Figure 2e and Table S1). Interestingly, thermal hysteresis was observed during the assembly and disassembly processes, indicating that the critical elongation temperatures are clearly determined as T_e' and T_e in the cooling and heating processes, respectively. As the heating and cooling rates decreased from 10 to 0.5 K/min, the T_e and T_e' values increased from 30 to 38 °C and from 4 to 12 °C, respectively. These results reveal that the supramolecular polymerization of *R*-TTI does not keep up with the rapid temperature changes under kinetic control.[59,60] By diluting the total concentration of *R*-TTI (c_T), a linear decrease in the T_e' was observed in the van't Hoff plot. From this analysis, the standard enthalpy ($\Delta H°$) and entropy ($\Delta S°$) were estimated to be −41.9 kJ mol^{-1} and −84.0 J mol^{-1} K^{-1}, respectively (Figure S26).

To investigate the effect of molecular level chirality on the supramolecular structure, X-ray scattering was performed on *N*-TTI and *R*-TTI assemblies. The difference in the crystal structure caused by the $\pi-\pi$ stacking in the achiral and chiral systems was analyzed using X-ray diffraction (XRD) measurements. The XRD pattern in its film state showed a single broad peak at approximately 20° corresponding to a spacing of 0.40 nm, resulting from the intermolecular distance between the stacked triphenylene moieties (Figure S27). Synchrotron small- and wide-angle X-ray scattering (SAXS and WAXS) experiments were also performed to investigate the crystalline phases and interatomic spacings in the unit cells. The *N*-TTI displayed diffraction peaks adopting a cubic geometry with the $Im\bar{3}m$ phase in the high-*q* region of the WAXS pattern (Figure S28a and Table S2).[61] The schematic illustration shows that the columns of *N*-TTI are arranged in a quasi-cubic geometry with a lattice size of 3.2 nm (Figure S28c). In the chiral system, the diffraction peaks corresponded to crystalline phases with a rectangular geometry and a *P*222 space group (Figure S28b and Table S3).[62,63] The size of the unit cell was determined based on the values obtained from the diffraction pattern (Figure S28d). Interestingly, the arrangement of *N*-TTI and *R*-TTI with imide bonds contrasts with that of triphenylene-based mesogens, which self-assemble into a hexagonal columnar geometry.[64,65] Because no diffraction peaks appeared in the low-*q* region of the SAXS pattern (Figure S29), it is estimated that *N*-TTI and *R*-TTI are cubic and complicated crystalline phases, respectively, based on the results obtained from the WAXS pattern.

To investigate the formation of radical species for TTI via the photoredox process, electron paramagnetic resonance (EPR) spectroscopy was performed using 5,5-dimethyl-1-pyrroline *N*-oxide (DMPO) as a spin-trapping reagent to detect short-lived radical species (Figure 3a). The radical-mediated structural variation process under light irradiation can be rapidly confirmed through CD measurement using *R*-TTI as a representative compound. The deoxygenated solution of *R*-TTI with DMPO was irradiated in situ in the EPR capillary at room temperature by using UV light (365 nm). When *R*-TTI was irradiated in isopropanol containing DMPO, EPR-detectable signals were observed (Figures 3b and S30). The highest EPR intensity was observed after 10 min of irradiation, which subsequently decreased. The simulation of the EPR spectra obtained at 5, 10, and 30 min of irradiation time based on the hyperfine splitting constants of DMPO radical adducts in the naphthalene diimides[66] was conducted to achieve detailed information from the spectra. Specifically, the simulated spectrum in Figure 3b contains contributions from two radical species identified as DMPO adducts with $C_3H_7O^\bullet$ (DMPO/$C_3H_7O^\bullet$) and $^\bullet C_3H_6OH$ (DMPO/$^\bullet C_3H_6OH$) radicals produced in isopropanol. It should be noted that the signals corresponding to the TTI$^{\bullet-}$ radical anions did not obtain, possibly due to the short lifetime of the radicals that are unable to detect in the EPR time scale. The calculated *g*-values and hyperfine splitting constants (a_N, a_H^β, and a_H^γ) are listed in Table S4. The DMPO/$C_3H_7O^\bullet$ adduct is the dominating radical species in all spectra (Figure 3c). The population of the entire radical species increases as the light irradiation time increases to 10 min, which then decreases because the amount of attenuation is greater than that of formation by the short-lived feature of the radicals. The relative ratio of the DMPO/$C_3H_7O^\bullet$ radical decreases over time, whereas that of the DMPO/$^\bullet C_3H_6OH$ radical increases. The amount of radical species produced by irradiation was 0.113 mM (38%) and 0.222 mM (74%) with respect to *R*-TTI at 5 and 10 min, respectively, based on the calibration curve constructed using the EPR signals of 2,2,6,6-tetramethylpiperidine 1-oxyl (TEMPO) as a standard (Figure S31). The proposed mechanisms for radical formation during the UV irradiation of *R*-TTI in isopropanol are shown in Figure 3d. The radical cation TTI$^{\bullet+}$ and radical anion TTI$^{\bullet-}$ are photogenerated directly from a singlet state excimer of TTI dimers because the excited state TTI can be quenched through electron transfer from TTI in the ground state. The radical cation TTI$^{\bullet+}$ acts as an oxidant and can be reduced to TTI by oxidizing isopropanol to form the $C_3H_7O^\bullet$ radical. The photogenerated triplet state can be self-quenched, producing the radical cation TTI$^{\bullet+}$ and radical anion TTI$^{\bullet-}$. Furthermore, the TTI triplet can be quenched by an electron transfer from

https://doi.org/10.1021/acs.macromol.3c01189
Macromolecules XXXX, XXX, XXX−XXX

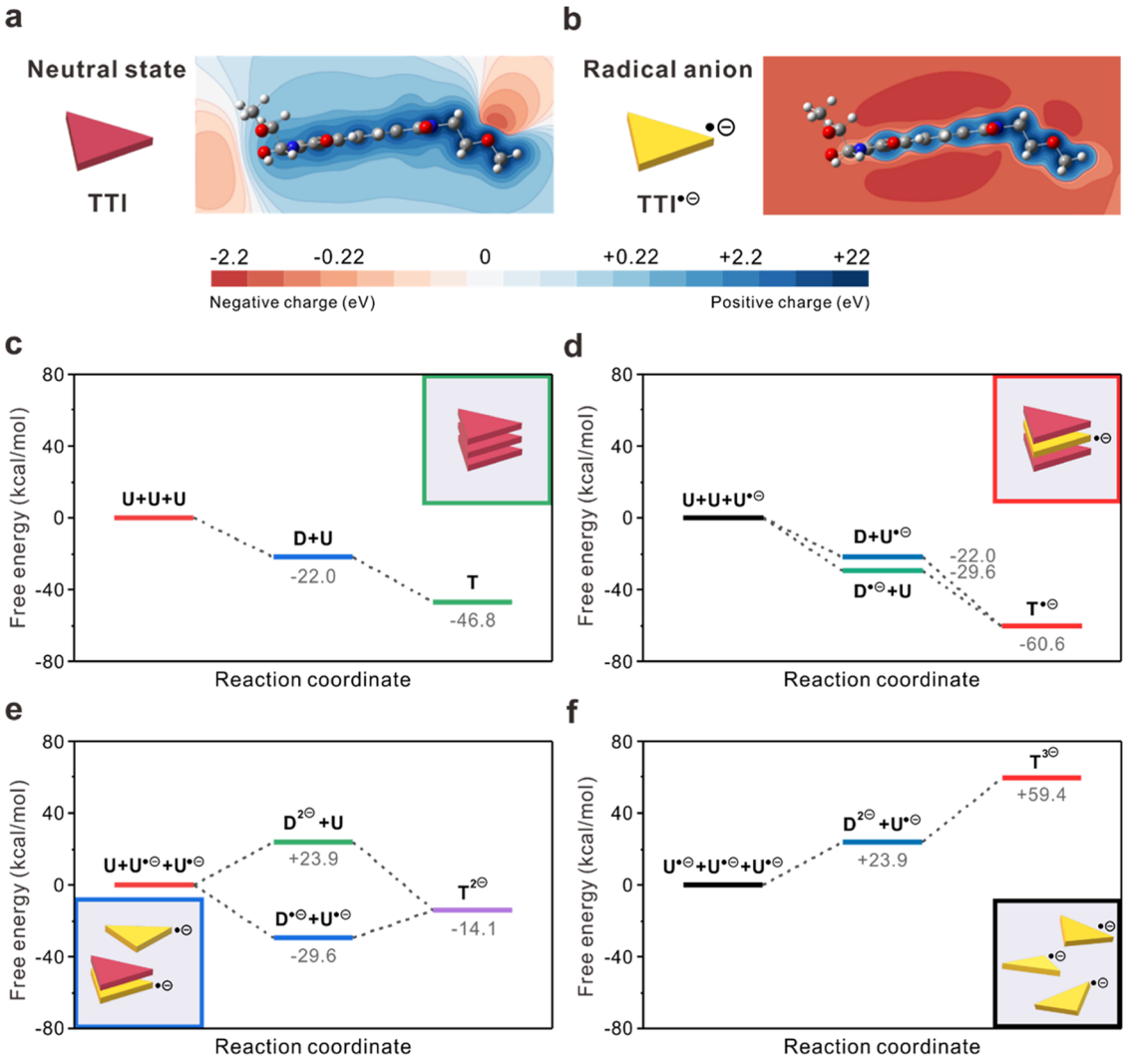

Figure 4. Electrostatic potential contour diagrams taken from the side view of (a) neutral and (b) radical anion of simplified TTI. Gibbs free-energy profiles for TTI assemblies (i.e., trimers) in (c) three neutral unimers, (d) two neutral and one radical anion unimers, (e) one neutral and two radical anion unimers, and (f) three radical anion unimers. U, D, and T indicate the unimer, dimer, and trimer, respectively. The inset image shows the most stable state in the corresponding combination. The molecular structure of TTI was simplified by substituting the side chains with methoxy groups, and optimized geometries of TTI unimer, dimer, and trimer are summarized in Tables S5−S7. Refer to the Supporting Information for details.

isopropyl alcohol, leading to the formation of $TTI^{\bullet-}$ with $C_3H_7O^{\bullet}$ and $^{\bullet}C_3H_6OH$ radicals.

Furthermore, the generation of radical anions for *R*-TTI was detected by using cytochrome c as a model compound. Cytochrome c is a small redox protein involved in the mitochondrial electron-transfer system, which includes a heme group where the central iron atom can be reduced from the Fe^{3+} to the Fe^{2+} state. Free radicals from organic redox molecules, such as naphthalene diimide derivatives, can be used to reduce cytochrome c.[45] The absorption spectra of an aqueous solution containing cytochrome c and *R*-TTI were measured with respect to the UV irradiation time. A red shift in the Soret band at 414 nm and new absorption bands at 520 and 549 nm were observed (Figure S32a), which are typical spectral changes of the reduced cytochrome c. The reduction kinetics of cytochrome c were investigated by monitoring the absorption band at 549 nm under light irradiation. As shown in Figure S32b, cytochrome c was fully reduced in 60 s. These results suggest that the photogenerated transient species are derived from TTI via an imide radical anion.

The effect of the radical anion $TTI^{\bullet-}$ due to light irradiation on the self-assembly process was investigated via CD measurement. After the unimer solutions of *R*-TTI were irradiated with UV light, the self-assembly was facilitated by cooling the solutions to −10 °C. This process leads to the formation of $TTI^{\bullet-}$, while monitoring its supramolecular polymerization behavior. When the chiral monomer (*R*-TTI) is irradiated with light, the resulting radical anion in Figure 3e exhibits a CD signal in the range of 280−320 nm, indicating the presence of molecular chirality. When the unimer was irradiated with UV light, the CD intensity corresponding to the supramolecular polymers was reduced with respect to the irradiation time, implying that the radical anion $TTI^{\bullet-}$ prevents the self-assembly of the unimer (Figure 3e). The decrease in the CD intensity saturated at 10 min when the population of radical species was the highest. The self-assembly hardly proceeds when the production of the radical anions is saturated as confirmed by AFM measurement (Figures 3a and S33). It is expected that fiber growth was suppressed due to the electrostatic repulsion between radical anions. Furthermore,

https://doi.org/10.1021/acs.macromol.3c01189
Macromolecules XXXX, XXX, XXX−XXX

radical species were generated in 2-propanol, the assembly solvent, which could have restricted the fiber growth due to changes in the self-assembly environment. The T_e' values of *R*-TTI in the cooling processes were reduced from 4 to 0 °C with irradiation time, resulting from limited fiber growth (Figure S34). On the other hand, when the supramolecular polymer was irradiated with UV light, the CD intensity hardly changed with irradiation time (Figure 3f). The red shift in the Soret band and new absorption bands at 520 and 549 nm in the absorption spectra measured at 25 °C indicate that radical anion $TTI^{\bullet-}$ was generated in the unimer state upon light irradiation (Figure S35a). However, little change was observed in the absorption spectrum measured at −10 °C under light irradiation (Figure S35b). Therefore, it can be assumed that the formation of radical anions is difficult because the reaction between the alcohol solvent and imide bonds does not occur efficiently in the supramolecular state due to strong intermolecular interactions. Another hypothesis states that the fast coupling between radical anions occurs due to the intermolecular interactions,[51,52,67−69] resulting in no disassembly of the supramolecular polymers. Furthermore, when the *N*-TTI unimer was irradiated with UV light, the absorbance decreased with irradiation time, indicating limited growth (Figure S36).

UV light irradiation of the unimer solution caused the formation of radical anions in aromatic imide units, which limited continuous growth by generating inactive building blocks. When the critical time was exceeded, the self-assembly did not proceed due to the completely deactivated unimers. Conversely, the irradiation of the supramolecular polymer solution had no critical influence on the self-assembly process because the light absorption was restrained due to its aggregated state. Although the phototriggered deactivation of unimers via a reduction reaction was the first example, the reactivation of the radical anion into the original unimer form could not be realized via an oxidation reaction possibly because the resulting structural variation could not be recovered owing to the reactivity of the active radical species (Figure S37).

To demonstrate the limited growth that occurs due to the unfavorable electrostatic repulsion between radical anions, the electrostatic potential and Gibbs free energy of the neutral state as well as radical anion were approximated based on density functional theory (DFT) using ωB97XD functional and 6-31G(d) basis sets (see details in the Supporting Information). As shown in the electrostatic potential contour diagrams of Figure 4a,b, radical anion $TTI^{\bullet-}$ has a high negative electrostatic potential of −2.2 eV on the aromatic core unit compared to that of neutral TTI, which significantly affects the self-assembly. To further understand the impact of radical anion on self-assembly, Gibbs free-energy profiles were calculated for TTI assemblies consisting of various combinations of neutral and radical anion unimers. Figure 4c,d shows that the Gibbs free energy gradually decreased as TTI assemblies proceeded due to π−π stacking interactions in the neutral state and the state with one radical anion and two neutral unimers, indicating the self-assembly (e.g., trimerization), is energetically favored. However, when there are two radical anions and one neutral unimer, dimerization becomes more stable than trimerization (Figure 4e). Furthermore, the self-assembly process in the state with only a radical anion is energetically unfavorable due to electrostatic repulsion between radical anions (Figure 4f). DFT results suggest that the molecular interactions become less favorable as the ratio of radical anions increases, which is in good agreement with the limited growth with respect to UV irradiation time.

Finally, chiral sensing experiments were conducted to explore the potential applicability of chiral supramolecular polymers for the detection of chiral aromatic compounds (Figure S38). Specifically, *R*/*S*-methylbenzylamine and benzylamine were used as the chiral and achiral quenchers, respectively. Due to the fluorescent behavior of the triphenylene moiety, all TTI assemblies acted as sensors utilizing a fluorescence quenching mechanism.[70] The introduction of quenchers induces a decrease in the fluorescence intensity of TTI, which is attributed to the formation of charge-transfer complexes. Notably, the *R*/*S*-TTI assemblies exhibited a higher quenching efficiency for analytes with the same chirality than for those with opposite chirality. Consequently, the chiral quenchers could be selectively detected depending on the chirality of the supramolecular polymer.

3. CONCLUSIONS

C_3-symmetric TTI as a new aromatic imide compound comprised a conjugated triphenylene core and three elongated OEG side chains connected via imide linkages. The supramolecular polymers were obtained by slowly cooling the solution of TTI unimers. Through π−π stacking and hydrophilic/hydrophobic interactions, TTI formed long fibrous supramolecular polymers, which was confirmed by AFM and TEM observations. The fibers assembled from the *R*-TTI unimer were twisted at some point along the main axis. The molecular packing structures of *N*-TTI and *R*-TTI were assigned to cubic and rectangular phases, respectively, as determined by WAXS measurements.

Notably, UV light irradiation formed radical anions by reducing the *R*-TTI unimers. Based on the experimental and simulated EPR results, it was possible to indirectly prove the generation of radical anions in the *R*-TTI unimer through the presence of radical signals from the alcohol solvent. The formation of radical anions induced structural changes, resulting in the limited growth of the fibrous assemblies of *R*-TTI. When UV light was irradiated on the *R*-TTI assemblies, the supramolecular structure was maintained, owing to its tight intermolecular interactions. Our study elucidated that the dynamic chiral supramolecular assembly can be realized in a new C_3-symmetric aromatic imide compound by the radical anions generated upon UV light irradiation. We anticipate this study provides a new platform for designing and understanding phototriggered supramolecular systems.

■ ASSOCIATED CONTENT

Supporting Information

The Supporting Information is available free of charge at https://pubs.acs.org/doi/10.1021/acs.macromol.3c01189.

Detailed experimental procedures; ^1H, ^{13}C, DOSY NMR, ESI-MS, and FT-IR spectra of the unimers; supramolecular polymerization of *S*-TTI; additional AFM, TEM, and XRD data of *N*-TTI and *R*-TTI; EPR data of *R*-TTI and TEMPO; UV−vis absorbance spectra of *R*-TTI with cytochrome c; DFT simulation model; and fluorescence intensity of *R*-TTI, *S*-TTI, and *N*-TTI assemblies for chiral sensing experiment (PDF)

https://doi.org/10.1021/acs.macromol.3c01189
Macromolecules XXXX, XXX, XXX−XXX

AUTHOR INFORMATION

Corresponding Author

Byeong-Su Kim − *Department of Chemistry, Yonsei University, Seoul 03722, Republic of Korea;* orcid.org/0009-0006-9922-8081; Email: bskim19@yonsei.ac.kr

Authors

Namhee Kim − *Department of Chemistry, Yonsei University, Seoul 03722, Republic of Korea;* orcid.org/0000-0003-2214-5588

Jun Su Kang − *Department of Chemistry, Korea Advanced Institute of Science and Technology (KAIST), Daejeon 34141, Republic of Korea;* orcid.org/0000-0003-1417-3482

Taesuk Jun − *Department of Chemical and Biomolecular Engineering, Yonsei University, Seoul 03722, Republic of Korea*

Jong-Min Suh − *Department of Chemistry, Korea Advanced Institute of Science and Technology (KAIST), Daejeon 34141, Republic of Korea*

Deok-Ho Roh − *Department of Chemistry, Ulsan National Institute of Science and Technology (UNIST), Ulsan 44919, Republic of Korea*

Won-Woo Park − *Department of Chemistry, Ulsan National Institute of Science and Technology (UNIST), Ulsan 44919, Republic of Korea;* orcid.org/0000-0001-9602-6018

Oh-Hoon Kwon − *Department of Chemistry, Ulsan National Institute of Science and Technology (UNIST), Ulsan 44919, Republic of Korea;* orcid.org/0000-0001-7114-8617

Tae-Hyuk Kwon − *Department of Chemistry, Ulsan National Institute of Science and Technology (UNIST), Ulsan 44919, Republic of Korea;* orcid.org/0000-0002-1633-6065

Mi Hee Lim − *Department of Chemistry, Korea Advanced Institute of Science and Technology (KAIST), Daejeon 34141, Republic of Korea;* orcid.org/0000-0003-3377-4996

Du Yeol Ryu − *Department of Chemical and Biomolecular Engineering, Yonsei University, Seoul 03722, Republic of Korea;* orcid.org/0000-0002-0929-7934

Myungeun Seo − *Department of Chemistry, Korea Advanced Institute of Science and Technology (KAIST), Daejeon 34141, Republic of Korea;* orcid.org/0000-0002-5218-3502

Complete contact information is available at: https://pubs.acs.org/10.1021/acs.macromol.3c01189

Notes

The authors declare no competing financial interest.

ACKNOWLEDGMENTS

This work was supported by the National Research Foundation of Korea (NRF-2018R1A5A1025208, NRF-2021R1A2C3004978, NRF-2022R1A6A3A13053831, and NRF-2022R1A3B1077319). The EPR experiment was supported by the Institute for Basic Science (IBS-R010-D1) in Korea. The authors thank the EPR lab at KBSI Western Seoul Center.

REFERENCES

(1) Stupp, S. I.; Palmer, L. C.; Sai, H. Crystalline supramolecular polymers: dynamics, chirality, and function. *Isr. J. Chem.* **2021**, *61*, 873−883, DOI: 10.1002/ijch.202100104.

(2) Bailey, J.; Chrysostomou, A.; Hough, J. H.; Gledhill, T. M.; McCall, A.; Clark, S.; Ménard, F.; Tamura, M. Circular polarization in star- formation regions: implications for biomolecular homochirality. *Science* **1998**, *281*, 672−674.

(3) Takahashi, R.; Nishimichi, T.; Namikawa, T.; Taruya, A.; Kayo, I.; Osato, K.; Kobayashi, Y.; Shirasaki, M. Fitting the nonlinear matter bispectrum by the halofit approach. *Astrophys. J.* **2020**, *895*, No. 113, DOI: 10.3847/1538-4357/ab908d.

(4) Wang, H.; Yong, X.; Huang, H.; Yu, H.; Wu, Y.; Deng, J. Chiral, thermal-responsive hydrogels containing helical hydrophilic polyacetylene: preparation and enantio-differentiating release ability. *Polym. Chem.* **2019**, *10*, 1780−1786.

(5) Liu, J.; Yuan, F.; Ma, X.; Auphedeous, D.-i. Y.; Zhao, C.; Liu, C.; Shen, C.; Feng, C. The cooperative effect of both molecular and supramolecular chirality on cell adhesion. *Angew. Chem., Int. Ed.* **2018**, *57*, 6475−6479.

(6) Mao, B.; Fañanás-Mastral, M.; Feringa, B. L. Catalytic asymmetric synthesis of butenolides and butyrolactones. *Chem. Rev.* **2017**, *117*, 10502−10566.

(7) Jin, Q.; Zhang, L.; Cao, H.; Wang, T.; Zhu, X.; Jiang, J.; Liu, M. Self-assembly of copper(II) ion-mediated nanotube and its supramolecular chiral catalytic behavior. *Langmuir* **2011**, *27*, 13847−13853.

(8) Raynal, M.; Portier, F.; van Leeuwen, P. W. N. M.; Bouteiller, L. Tunable asymmetric catalysis through ligand stacking in chiral rigid rods. *J. Am. Chem. Soc.* **2013**, *135*, 17687−17690.

(9) Liu, L.; Yang, Y.; Wang, Y.; Adil, M. A.; Zhao, Y.; Zhang, J.; Chen, K.; Deng, D.; Zhang, H.; Amin, K.; Wu, Y.; Zhang, Y.; Wei, Z. Building supramolecular chirality in bulk heterojunctions enables amplified dissymmetry current for high-performing circularly polarized light detection. *ACS Mater. Lett.* **2022**, *4*, 401−409.

(10) Yang, Y.; da Costa, R. C.; Fuchter, M. J.; Campbell, A. J. Circularly polarized light detection by a chiral organic semiconductor transistor. *Nat. Photonics* **2013**, *7*, 634−638.

(11) Gilot, J.; Abbel, R.; Lakhwani, G.; Meijer, E. W.; Schenning, A. P. H. J.; Meskers, S. C. J. Polymer photovoltaic cells sensitive to the circular polarization of light. *Adv. Mater.* **2010**, *22*, E131−E134.

(12) Schulz, M.; Balzer, F.; Scheunemann, D.; Arteaga, O.; Lützen, A.; Meskers, S. C. J.; Schiek, M. Chiral excitonic organic photodiodes for direct detection of circular polarized light. *Adv. Funct. Mater.* **2019**, *29*, No. 1900684.

(13) Xu, F.; Crespi, S.; Pacella, G.; Fu, Y.; Stuart, M. C. A.; Zhang, Q.; Portale, G.; Feringa, B. L. Dynamic control of a multistate chiral supramolecular polymer in water. *J. Am. Chem. Soc.* **2022**, *144*, 6019−6027.

(14) Baker, M. B.; Albertazzi, L.; Voets, I. K.; Leenders, C. M. A.; Palmans, A. R. A.; Pavan, G. M.; Meijer, E. W. Consequences of chirality on the dynamics of a water-soluble supramolecular polymer. *Nat. Commun.* **2015**, *6*, No. 6234.

(15) Kim, J.; Lee, J.; Kim, W. Y.; Kim, H.; Lee, S.; Lee, H. C.; Lee, Y. S.; Seo, M.; Kim, S. Y. Induction and control of supramolecular chirality by light in self-assembled helical nanostructures. *Nat. Commun.* **2015**, *6*, No. 6959.

(16) Kang, J. S.; Kim, N.; Kim, T.; Seo, M.; Kim, B.-S. Circularly polarized light-driven supramolecular chirality. *Macromol. Rapid Commun.* **2022**, *43*, No. 2100649.

(17) George, S. J.; Tomović, Ž.; Schenning, A. P. H. J.; Meijer, E. W. Insight into the chiral induction in supramolecular stacks through preferential chiral solvation. *Chem. Commun.* **2011**, *47*, 3451−3453.

(18) Ślęczkowski, M. L.; Mabesoone, M. F. J.; Ślęczkowski, P.; Palmans, A. R. A.; Meijer, E. W. Competition between chiral solvents and chiral monomers in the helical bias of supramolecular polymers. *Nat. Chem.* **2021**, *13*, 200−207.

(19) Fernández, Z.; Fernández, B.; Quiñoá, E.; Freire, F. Merging supramolecular and covalent helical polymers: four helices within a single scaffold. *J. Am. Chem. Soc.* **2021**, *143*, 20962−20969.

(20) Salikolimi, K.; Praveen, V. K.; Sudhakar, A. A.; Yamada, K.; Horimoto, N. N.; Ishida, Y. Helical supramolecular polymers with rationally designed binding sites for chiral guest recognition. *Nat. Commun.* **2020**, *11*, No. 2311.

(21) Mori, T.; Akagi, K. Superhelix structure in helical conjugated polymers synthesized in an asymmetric reaction field. *Macromolecules* **2013**, *46*, 6699−6711.
(22) Li, F.; Li, X.; Wang, Y.; Zhang, X. Trismaleimide dendrimers: helix-to-superhelix supramolecular transition accompanied by white-light emission. *Angew. Chem., Int. Ed.* **2019**, *58*, 17994−18002.
(23) Wen, T.; Shen, H.-Y.; Wang, H.-F.; Mao, Y.-C.; Chuang, W.-T.; Tsai, J.-C.; Ho, R.-M. Controlled handedness of twisted lamellae in banded spherulites of isotactic poly(2-vinylpyridine) as induced by chiral dopants. *Angew. Chem., Int. Ed.* **2015**, *54*, 14313−14316.
(24) Li, M.-C.; Wang, H.-F.; Chiang, C.-H.; Lee, Y.-D.; Ho, R.-M. Lamellar-twisting-induced circular dichroism of chromophore moieties in banded spherulites with evolution of homochirality. *Angew. Chem., Int. Ed.* **2014**, *53*, 4450−4455.
(25) Zhang, Y.; Xia, B.; Hu, Y.; Zhu, Q.; Lin, X.; Wu, Q. Enantiocomplementary chiral polyhydroxyenoate: chemoenzymatic synthesis and helical structure control. *ACS Macro Lett.* **2019**, *8*, 1188−1193.
(26) Schreiber, R.; Luong, N.; Fan, Z.; Kuzyk, A.; Nickels, P. C.; Zhang, T.; Smith, D. M.; Yurke, B.; Kuang, W.; Govorov, A. O.; Liedl, T. Chiral plasmonic DNA nanostructures with switchable circular dichroism. *Nat. Commun.* **2013**, *4*, No. 2948.
(27) Duan, P.; Li, Y.; Li, L.; Deng, J.; Liu, M. Multiresponsive chiroptical switch of an azobenzene-containing lipid: solvent, temperature, and photoregulated supramolecular chirality. *J. Phys. Chem. B* **2011**, *115*, 3322−3329.
(28) Li, Y.; Wang, T.; Liu, M. Gelating-induced supramolecular chirality of achiral porphyrins: chiroptical switch between achiral molecules and chiral assemblies. *Soft Matter* **2007**, *3*, 1312−1317.
(29) Liu, G.; Sheng, J.; Teo, W. L.; Yang, G.; Wu, H.; Li, Y.; Zhao, Y. Control on dimensions and supramolecular chirality of self-assemblies through light and metal ions. *J. Am. Chem. Soc.* **2018**, *140*, 16275−16283.
(30) Niu, D.; Jiang, Y.; Ji, L.; Ouyang, G.; Liu, M. Self-assembly through coordination and π-stacking: controlled switching of circularly polarized luminescence. *Angew. Chem., Int. Ed.* **2019**, *58*, 5946−5950.
(31) Cai, Y.; Guo, Z.; Chen, J.; Li, W.; Zhong, L.; Gao, Y.; Jiang, L.; Chi, L.; Tian, H.; Zhu, W.-H. Enabling light work in helical self-assembly for dynamic amplification of chirality with photoreversibility. *J. Am. Chem. Soc.* **2016**, *138*, 2219−2224.
(32) Zhang, L.; Wang, H.-X.; Li, S.; Liu, M. Supramolecular chiroptical switches. *Chem. Soc. Rev.* **2020**, *49*, 9095−9120.
(33) Iftime, G.; Labarthet, F. L.; Natansohn, A.; Rochon, P. Control of chirality of an azobenzene liquid crystalline polymer with circularly polarized light. *J. Am. Chem. Soc.* **2000**, *122*, 12646−12650.
(34) Kim, M.-J.; Shin, B.-G.; Kim, J.-J.; Kim, D.-Y. Photoinduced supramolecular chirality in amorphous azobenzene polymer films. *J. Am. Chem. Soc.* **2002**, *124*, 3504−3505.
(35) Wang, L.; Yin, L.; Zhang, W.; Zhu, X.; Fujiki, M. Circularly polarized light with sense and wavelengths to regulate azobenzene supramolecular chirality in optofluidic medium. *J. Am. Chem. Soc.* **2017**, *139*, 13218−13226.
(36) Choi, S.-W.; Izumi, T.; Hoshino, Y.; Takanishi, Y.; Ishikawa, K.; Watanabe, J.; Takezoe, H. Circular-polarization-induced enantiomeric excess in liquid crystals of an achiral, bent-shaped mesogen. *Angew. Chem., Int. Ed.* **2006**, *45*, 1382−1385.
(37) Manaka, T.; Hideki, K.; Yuki, O.; Gang, Z.; Mitsumasa, I. Preparation of chiral polydiacetylene film from achiral monomers using circularly polarized light. *Chem. Lett.* **2006**, *35*, 1028−1029.
(38) Yang, G.; Han, L.; Jiang, H.; Zou, G.; Zhang, Q.; Zhang, D.; Wang, P.; Ming, H. Enantioselective synthesis of helical polydiacetylenes in the visible light region. *Chem. Commun.* **2014**, *50*, 2338−2340.
(39) Xu, Y.; Yang, G.; Xia, H.; Zou, G.; Zhang, Q.; Gao, J. Enantioselective synthesis of helical polydiacetylene by application of linearly polarized light and magnetic field. *Nat. Commun.* **2014**, *5*, No. 5050.
(40) He, C.; Yang, G.; Kuai, Y.; Shan, S.; Yang, L.; Hu, J.; Zhang, D.; Zhang, Q.; Zou, G. Dissymmetry enhancement in enantioselective synthesis of helical polydiacetylene by application of superchiral light. *Nat. Commun.* **2018**, *9*, No. 5117.
(41) Lü, B.; Chen, Y.; Li, P.; Wang, B.; Müllen, K.; Yin, M. Stable radical anions generated from a porous perylenediimide metal-organic framework for boosting near-infrared photothermal conversion. *Nat. Commun.* **2019**, *10*, No. 767, DOI: 10.1038/s41467-019-08434-4.
(42) Liu, H.; Yin, G.; Li, Q.; Liu, G.; Pu, S.; Zhang, H. Visible-light-triggered generation of persistent radical anions from perylenediimides: a substituent effect and potential application in photocatalytic reduction of Ag^+. *Dyes Pigm.* **2019**, *165*, 319−326.
(43) Gong, H.-X.; Cao, Z.; Li, M.-H.; Liao, S.-H.; Lin, M.-J. Photoexcited perylene diimide radical anions for the reduction of aryl halides: a bay-substituent effect. *Org. Chem. Front.* **2018**, *5*, 2296−2302.
(44) Zeman, C. J. I. V.; Kim, S.; Zhang, F.; Schanze, K. S. Direct observation of the reduction of aryl halides by a photoexcited perylene diimide radical anion. *J. Am. Chem. Soc.* **2020**, *142*, 2204−2207.
(45) Song, Q.; Li, F.; Wang, Z.; Zhang, X. A supramolecular strategy for tuning the energy level of naphthalenediimide: promoted formation of radical anions with extraordinary stability. *Chem. Sci.* **2015**, *6*, 3342−3346.
(46) Saha, M.; Bandyopadhyay, S. Stimuli responsive stable radical anion for conductance switching. *J. Phys. Chem. C* **2021**, *125*, 6427−6432.
(47) Zhao, X.; Liu, F.; Zhao, Z.; Karoui, H.; Bardelang, D.; Ouari, O.; Liu, S. Effects of cucurbit[n]uril (n = 7, 8, 10) hosts on the formation and stabilization of a naphthalenediimide (NDI) radical anion. *Org. Biomol. Chem.* **2018**, *16*, 3809−3815.
(48) Caby, S.; Bouchet, L. M.; Argüello, J. E.; Rossi, R. A.; Bardagi, J. I. Excitation of radical anions of naphthalene diimides in consecutive- and electro-photocatalysis. *ChemCatChem* **2021**, *13*, 3001−3009.
(49) Leira-Iglesias, J.; Tassoni, A.; Adachi, T.; Stich, M.; Hermans, T. M. Oscillations, travelling fronts and patterns in a supramolecular system. *Nat. Nanotechnol.* **2018**, *13*, 1021−1027.
(50) Jalani, K.; Das, A. D.; Sasmal, R.; Agasti, S. S.; George, S. J. Transient dormant monomer states for supramolecular polymers with low dispersity. *Nat. Commun.* **2020**, *11*, No. 3967.
(51) Penneau, J. F.; Stallman, B. J.; Kasai, P. H.; Miller, L. L. An imide anion radical that dimerizes and assembles into.pi.-stacks in solution. *Chem. Mater.* **1991**, *3*, 791−796.
(52) Penneau, J.-F.; Miller, L. L. An imide radical anion which assembles into π-stacks in solution. *Angew. Chem., Int. Ed.* **1991**, *30*, 986−987.
(53) Wang, Y.; Jiang, Y.; Zhu, X.; Liu, M. Significantly boosted and inversed circularly polarized luminescence from photogenerated radical anions in dipeptide naphthalenediimide assemblies. *J. Phys. Chem. Lett.* **2019**, *10*, 5861−5867.
(54) Kumar, S.; Ajayakumar, M. R.; Hundal, G.; Mukhopadhyay, P. Extraordinary stability of naphthalenediimide radical ion and its ultra-electron-deficient precursor: strategic role of the phosphonium group. *J. Am. Chem. Soc.* **2014**, *136*, 12004−12010.
(55) Lee, S.-H.; Oh, B. M.; Hong, C. Y.; Jung, S.-K.; Park, S.-H.; Jeon, G. G.; Kwon, Y.-W.; Jang, S.; Lee, Y.; Kim, D.; Kim, J. H.; Kwon, O. P. Gas-induced ion-free stable radical anion formation of organic semiconducting solids as highly gas-selective probes. *ACS Appl. Mater. Interfaces* **2019**, *11*, 35904−35913.
(56) Hartlieb, M.; Mansfield, E. D. H.; Perrier, S. A guide to supramolecular polymerizations. *Polym. Chem.* **2020**, *11*, 1083−1110.
(57) Würthner, F.; Kaiser, T. E.; Saha-Möller, C. R. J-aggregates: from serendipitous discovery to supramolecular engineering of functional dye materials. *Angew. Chem., Int. Ed.* **2011**, *50*, 3376−3410.
(58) Bricks, J. L.; Slominskii, Y. L.; Panas, I. D.; Demchenko, A. P. Fluorescent J-aggregates of cyanine dyes: basic research and applications review. *Methods Appl. Fluoresc.* **2018**, *6*, No. 012001.
(59) Ogi, S.; Stepanenko, V.; Sugiyasu, K.; Takeuchi, M.; Würthner, F. Mechanism of self-assembly process and seeded supramolecular

https://doi.org/10.1021/acs.macromol.3c01189
Macromolecules XXXX, XXX, XXX−XXX

polymerization of perylene bisimide organogelator. *J. Am. Chem. Soc.* **2015**, *137*, 3300−3307.
(60) Xu, F.; Crespi, S.; Pfeifer, L.; Stuart, M. C. A.; Feringa, B. L. Mechanistic insight into supramolecular polymerization in water tunable by molecular geometry. *CCS Chem.* **2022**, *4*, 2212−2220.
(61) Sahoo, D.; Peterca, M.; Aqad, E.; Partridge, B. E.; Heiney, P. A.; Graf, R.; Spiess, H. W.; Zeng, X.; Percec, V. Hierarchical Self-Organization of Perylene Bisimides into Supramolecular Spheres and Periodic Arrays Thereof. *J. Am. Chem. Soc.* **2016**, *138*, 14798−14807.
(62) Percec, V.; Peterca, M.; Tadjiev, T.; Zeng, X.; Ungar, G.; Leowanawat, P.; Aqad, E.; Imam, M. R.; Rosen, B. M.; Akbey, U.; Graf, R.; Sekharan, S.; Sebastiani, D.; Spiess, H. W.; Heiney, P. A.; Hudson, S. D. Self-Assembly of Dendronized Perylene Bisimides into Complex Helical Columns. *J. Am. Chem. Soc.* **2011**, *133*, 12197−12219.
(63) Li, Y.-Y.; Wei, T.; Liu, C.; Zhang, Z.; Wu, L.-F.; Ding, M.; Yuan, S.; Zhu, J.; Zuo, J.-L. Integrating Tetrathiafulvalene and Nickel-Bis(dithiolene) Units into Donor-Acceptor Covalent Organic Frameworks for Stable and Efficient Photothermal Conversion. *Chem. - Eur. J.* **2023**, *29*, No. e202301048.
(64) Cammidge, A. N. The effect of size and shape variation in discotic liquid crystals based on triphenylene cores. *Philos. Trans. R. Soc., A* **2006**, *364*, 2697−2708, DOI: 10.1098/rsta.2006.1847.
(65) Osawa, T.; Kajitani, T.; Hashizume, D.; Ohsumi, H.; Sasaki, S.; Takata, M.; Koizumi, Y.; Saeki, A.; Seki, S.; Fukushima, T.; Aida, T. Wide-range 2D lattice correlation unveiled for columnarly assembled triphenylene hexacarboxylic esters. *Angew. Chem., Int. Ed.* **2012**, *51*, 7990−7993.
(66) Reszka, K. J.; Takayama, M.; Slk, R. H.; Chignell, C. F.; Salto, I. Photochemistry of naphthalene diimides: EPR study of free radical formation via photoredox process. *Photochem. Photobiol.* **2005**, *81*, 573−580.
(67) Cai, K.; Zhang, L.; Astumian, R. D.; Stoddart, J. F. Radical-pairing-induced molecular assembly and motion. *Nat. Rev. Chem.* **2021**, *5*, 447−465.
(68) Wu, Y.; Frasconi, M.; Gardner, D. M.; McGonigal, P. R.; Schneebeli, S. T.; Wasielewski, M. R.; Stoddart, J. F. Electron delocalization in a rigid cofacial naphthalene-1,8:4,5-bis-(dicarboximide) dimer. *Angew. Chem., Int. Ed.* **2014**, *53*, 9476−9481.
(69) Andric, G.; Boas, J. F.; Bond, A. M.; Fallon, G. D.; Ghiggino, K. P.; Hogan, C. F.; Hutchison, J. A.; Lee, M. A.-P.; Langford, S. J.; Pilbrow, J. R.; Troup, G. J.; Woodward, C. P. Spectroscopy of naphthalene diimides and their anion radicals. *Aust. J. Chem.* **2004**, *57*, 1011−1019.
(70) Gole, B.; Song, W.; Lackinger, M.; Mukherjee, P. S. Explosives sensing by using electron-rich supramolecular polymers: role of intermolecular hydrogen bonding in significant enhancement of sensitivity. *Chem. - Eur. J.* **2014**, *20*, 13662−13680.

https://doi.org/10.1021/acs.macromol.3c01189
Macromolecules XXXX, XXX, XXX−XXX